Published in final edited form as:
Cryobiology. 2010 February ; 60(1): 71–79. doi:10.1016/j.cryobiol.2008.11.008.

Computerized Planning of Prostate Cryosurgery Using Variable Cryoprobe Insertion Depth

Michael R. Rossi[1], **Daigo Tanaka**[2,†], **Kenji Shimada**[1,2], and **Yoed Rabin**[1,*]

[1]Department of Mechanical Engineering, Carnegie Mellon University, 5000 Forbes Ave., Pittsburgh, PA 15213

[2]Department of Biomedical Engineering, Carnegie Mellon University, 5000 Forbes Ave., Pittsburgh, PA 15213

Abstract

The current study presents a computerized planning scheme for prostate cryosurgery using a variable insertion-depth strategy. This study is a part of an ongoing effort to develop computerized tools for cryosurgery. Based on typical clinical practices, previous automated planning schemes have required that all cryoprobes be aligned at a single insertion depth. The current study investigates the benefit of removing this constraint, in comparison with results based on uniform insertion-depth planning as well as the so-called “pullback procedure”. Planning is based on the so-called “bubble-packing method”, and its quality is evaluated with bioheat transfer simulations. This study is based on five 3D prostate models, reconstructed from ultrasound imaging, and cryoprobe active length in the range of 15 mm to 35 mm. The variable insertion depth technique is found to consistently provide superior results when compared to the other placement methods. Furthermore, it is shown that both the optimal active length and the optimal number of cryoprobes vary among prostate models, based on the size and shape of the target region. Due to its low computational cost, the new scheme can be used to determine the optimal cryoprobe layout for a given prostate model in real time.

Keywords

Cryosurgery; Prostate; Computerized Planning; Bubble-Packing; Bioheat Transfer

1. Introduction

Cryosurgery, which is the destruction of undesired biological tissues by freezing, has been known as an invasive surgical technique since 1961, when Cooper and Lee invented the first modern, liquid nitrogen-based cryoprobe [4]. While minimally-invasive cryosurgery of the prostate was first introduced in the early 1980s, it was not until the early 1990s that technological developments allowed for the procedure to pass from the experimental stage to routine clinical practice [8]. Today, minimally-invasive prostate cryosurgery is performed

*Corresponding author: rabin@cmu.edu; Phone/Fax: 412 268 2204.
†Current address: WesternGeco – Schlumberger, Research & Engineering, 10001 Richmond Ave, Houston, TX 77042

with the application of multiple cryoprobes (in the shape of long hypodermic needles), strategically located in the region to be destroyed [5].

Currently, cryoprobe localization is an art held by the cryosurgeon, based on the surgeon's own experience and accepted practices. Once localized, cryoprobes are operated in a trial-and-error fashion, until the entire target volume is believed to be frozen. The cryosurgeon monitors the procedure by means of medical imaging—such as ultrasound or MRI [8,9,19,20]—and adjusts the cooling power of the individual cryoprobes accordingly, to best match the area to be treated with the developing frozen region. Once freezing begins, the cryoprobes cannot be relocated and, therefore, the outcome of the cryoprocedure is highly dependent upon the quality of the initial cryoprobe layout. Prostate cryosurgery often involves two freezing/thawing cycles, where the cryoprobes are retracted between cycles—also known as the "pullback procedure." The pullback procedure is aimed at improving the match between the area to be treated and the developing frozen region, but again, cryoprobes cannot be further relocated once freezing begins. Suboptimal cryoprobe placement may lead to portions of the target region being insufficiently cryotreated, cryoinjury to the healthy surrounding tissues, and elongated surgical operation, all of which affect the quality and the cost of the medical treatment. Computerized planning can help to alleviate these difficulties by identifying an optimal cryoprobe layout and providing close to real-time prediction of the resulting thermal field, with the match between the target region and the frozen region being one measure of the quality of planning. It is the development of planning strategies to identify the optimal cryoprobe layout which is the subject matter of the current paper.

A limited number of studies have addressed the need to develop computerized means to improve cryosurgical planning [2,3,6]. While these studies proposed various planning techniques, they were all associated with a high computational cost, thus preventing their practical application. Alternative methods for computerized planning of cryosurgery have been developed by the current research team, with the so-called "force-field analogy" being the most robust, but also the most computationally expensive of those developments [7,15]. More recently, the so-called "bubble-packing" method has been developed, with the objective of identifying the best initial condition for the force-field analogy method [23], by uniformly distributing bubbles in the target region, where the center of each bubble is the planned placement of a cryoprobe. The high quality of the cryoprobe layout at the end of the bubble-packing phase of planning, together with its relatively low computational cost, have made the need for a second-phase of planning (i.e., force-field analogy) debatable [22]. An experimental validation of bubble-packing-based planning has been presented recently, performed on a phantom material [18].

The current study is aimed at improving the bubble-packing method in two ways: by enabling variable insertion depth of cryoprobes and by optimizing various parameters associated with the bubble-packing scheme. The variable insertion depth concept is compared with two clinical practices: uniform insertion depth for all cryoprobes [24] and the pullback procedure, where two freezing cycles are executed and the cryoprobes are relocated backward between cycles [25]. In addition, results are compared for cryoprobes having active cooling lengths of 15 mm, 25 mm, and 35 mm. The current study was performed on the five prostate models reconstructed from ultrasound imaging in previous studies [22,26].

2. Mathematical Formulation

2.1. Bubble Packing

Computerized planning in the current study is based on the bubble packing method. While the principle of bubble packing are well documented in the literature [24,25], the method is

presented here in brief—for the completeness of presentation—with emphasis on the new modifications.

Bubble packing is a physically-based approach to search for an even distribution of a selected number of volumetric objects inside a given geometrical domain [21]. The bubble-packing scheme first generates ellipsoidal elements (or bubbles) inside the domain, where the ellipsoidal shape is taken as a first-order approximation of the early stage of freezing around an isolated cryoprobe. In addition, a stationary set of bubbles (boundary bubbles) are placed along the contour of the domain (i.e. the edge of the prostate), as well as along the urethral warmer. Next, van der Waals-like attractive and repulsive forces are simulated to move the non-stationary bubbles towards a force-balancing configuration. Consistent with previous studies [22–25], the van der Waals model is simplified to:

$$f(l)=\begin{cases} \alpha l^3+\beta l^3+\gamma l+\varepsilon & 0 \le l \le 1.5l_0 \\ 0 & 1.5l_0<l \end{cases} \quad (1)$$

subject to the following boundary conditions:

$$f(l_0)=f(1.5l_0)=0,\ f'(0)=0,\ f'(l_0)=-\kappa_0 \quad (2)$$

where l is the distance between two interacting bubbles, l_0 is the equilibrium distance if only two isolated bubbles are interacting, κ_0 is the a linear spring constant at distance l_0, and α, β, γ, and ε are the coefficients of the simplified van der Waals forcing function. The motion of bubbles towards a force-balancing configuration is simulated as a relaxation process of a second order system.

For the variable insertion depth cases presented in the current study, the bubble-packing algorithm is executed in two stages. In the first stage—in a somewhat similar process to the pullback method [25]—bubbles are equally distributed at two uniform but different insertion depths. In the second stage, all of the bubbles are allowed to move subject to intra-bubble forces, in a force relaxation process, until a minimum force-balancing configuration is reached.

For the current study, the size and shape of all bubbles are equal, and remain constant throughout the force relaxation process. The bubble dimensions are chosen based on the volume of the domain, the active length of the cryoprobes, and the number of cryoprobes being used. For a given target region, the bubble volume is chosen such that the total volume of bubbles equals the volume of the target region divided by a factor of 1.75. This factor was determined via trial-and-error, using all five prostate models presented in the current study. When a value less than 1.75 was used, bubbles tended to overpopulate the target region, resulting in a placement of cryoprobes too close to the center of the domain. Conversely, for factor values greater than 1.75, gaps between bubbles became too large, resulting in insufficient intra-bubble interaction and lower-quality cryoprobe placement. Hence, the bubble volume is given by:

$$V_B=\frac{V_T}{1.75n}=\frac{4}{3}\pi r_A {r_P}^2 \quad (3)$$

where V_B is the volume of one ellipsoidal bubble, V_T is the volume of the target region (i.e., the prostate), n is the number of bubbles, and r_A and r_P represent the bubble radii in the axial and perpendicular directions with respect to cryoprobe insertion.

While Eq. (3) provides one relationship between the ellipsoidal bubble radii, another relationship has been developed empirically, as follows:

$$\frac{2r_A - l_c}{2r_P - d_c} = \left(\frac{C_1}{l_c}\right)^{C_2} \tag{4}$$

where l_c and d_c are the length and the diameter of the cryoprobe, and C_1 and C_2 are empirical constants. The rationale for Eq. (4) is based on the assumption that a similarity relation exists between the cryoprobe dimensions and the ellipsoidal bubble dimensions. The numerator of the left hand side term represents the length difference between the bubble and the probe, and the denominator represents the diameter difference between the bubble and the probe. The right hand side term represents the relationship between the above differences ratio and the length of the cryoprobe. The optimal values for C_1 and C_2 were found to be 9 mm and 1.33, respectively, based on a series of bubble packing solutions with variable geometrical dimensions, including all five prostate models used in the current study.

Additional modifications made to the bubble-packing method in the current study: (i) attraction forces were eliminated, which means that the negative-value region of Eq. (1) is being truncated; (ii) a finite boundary bubble radius of 2 mm was selected (it was assumed infinitesimal in previous studies); (iii) the adaptive volume control of the bubbles was turned off; and (iv) a fixed bubble shape was selected, as discussed above, rather than using a fixed bubble axis ratio [24]. While the above set of modifications yields a higher-quality cryoprobe layout for the variable insertion depth case, it is assumed that the bubble packing parameters can be further optimized.

2.2. Bioheat Transfer Simulation

The classical bioheat equation [10] is used to simulate the heat transfer process during prostate cryosurgery:

$$C\frac{\partial T}{\partial t} = \nabla \cdot (k\nabla T) + \dot{w}_b C_b (T_b - T) + \dot{q}_{met} \tag{5}$$

where C is the volumetric specific heat of the tissue, T is the temperature, t is the time, k is the thermal conductivity of the tissue, $\dot{w}_b$ is the blood perfusion volumetric flow rate per unit volume of tissue, C_b is the volumetric specific heat of the blood, T_b is the blood temperature entering the thermally treated area, and q_{met} is the metabolic heat generation. Note that metabolic heat generation is typically negligible compared to the heating effect of blood perfusion [13], and is neglected in this study. The physical properties used for the current study are listed in Table 1.

The blood perfusion value in the unfrozen region, listed in Table 1, and the step-like change in the blood-perfusion rate around freezing represent the worst-case scenario in terms of transient effects. In practice, one would expect a gradual decrease in blood flow with the decreasing temperature, potentially leading to complete stasis before the freezing temperature is achieved. To the best of knowledge of the authors, the actual temperature dependency of blood perfusion in the prostate is unknown, while insight with regard to possible temperature dependency relations and extreme blood-perfusion rates in other tissues can be found in [13]. The uncertainty in blood perfusion rate can contribute to the uncertainty in predicting the freezing front location within a few percent [13]; this uncertainty is not taken into account in the current study. A detailed discussion concerning

the propagation of uncertainty in measurement into heat transfer simulations with application to cryosurgery is given in [14].

For the solution of the phase-change problem, it is assumed that the specific heat in Eq. (5) is an effective property within the phase transition temperature range of −22°C to 0°C (if the tissue is first-order approximated as an NaCl solution), where a detailed discussion about the application of the effective specific heat to phase change problems is given in [12]. The numerical scheme applied in the current study is based on a finite difference formulation of Eq. (5), and utilizes variably sized grid regions and time steps to meet the specific requirement of short runtime for clinical applications [17]. Recently, this scheme has been validated experimentally [16].

Consistent with the thermal analysis presented in [17], the simulated domain in the current study has a transversal cross-sectional area of 3.5 times larger than the largest cross-sectional area of the specific prostate model, and the length of the domain is set to be 1.5 times that of the same prostate model. These dimensions satisfy an underlying assumption that the human body behaves as an infinite domain in the thermal sense, when compared with the prostate size. The initial temperature throughout the simulated domain is set to the normal core-body temperature of 37°C. Two separate grid sizes are used throughout the simulated domain (1 mm and 3 mm), where the 1 mm grids are used around the cryoprobes and the urethral warmer.

The cross-section of each cryoprobe used in the current study is represented as 1 mm × 1 mm square; their perimeter is equivalent to that of a circular cryoprobe having a diameter of 1.3 mm. Simplifying the circular cryoprobe to be rectangular for the purpose of heat transfer simulations in the current study is deemed appropriate since the area of the active surface of the cryoprobe is the dominating parameter on heat transfer from the cryoprobe, rather than the diameter of the cryoprobe [17]. Furthermore, the typical volume of a frozen region is at least four orders of magnitude greater than that of the cryoprobe at the end of freezing, which makes the fine detail of the cryoprobe shape insignificant [17].

Applying typical parameters for a Joule-Thomson-based cryoprobe for cryosurgical simulation, the temperature of each cryoprobe is assumed to decrease linearly with temperature, starting with an initial value of 37°C and reaching −145°C in 30 sec; the cryoprobe temperature is assumed to be constant thereafter. While the power of a Joule-Thomson cryoprobe may be affected by the surroundings temperature, potentially leading to an interactive effect between cryoprobes when placed very close to one another, this effect has been excluded from the current analysis for demonstration purposes. This coupling effect bears no effect on the bubble-packing scheme, since it is taken as an external force (i.e., a boundary condition). In practice, this coupling effect is hardware specific, and its inclusion requires an experimental investigation of the cryosurgery system. Without affecting the generality of the methodology developed in the current study, the characterization of the above-mentioned coupling effect is a task left to the reduce-to-practice stage of planning.

2.3. Planning Objective

The objective for a cryosurgical procedure is to maximize tissue destruction internal to the target region while minimizing freezing injury to surrounding tissues. In the current study, the target region is defined as the entire prostate, excluding the urethra. In the absence of more detailed clinical requirements, the aim for planning is to lower the temperature of the entire target region below a specific temperature threshold determined by the clinician, while maintaining the temperature of the surrounding tissues above it. For this purpose, the defect-region concept is applied [7], where a defect is defined as tissue outside of the target

region with temperatures below the temperature threshold for planning (i.e., external defect), or tissue inside the target region with temperatures above the same temperature threshold (i.e., internal defect). Consistent with previous studies [7,15], the −22°C isotherm has been selected in the current study for demonstration purposes, since it represents both the lower boundary of phase transition in biological tissues (modeled as an NaCl solution) and the mid-range temperature between the onset of freezing and the so-called “lethal temperature” (frequently taken as −45°C by urologists).

The overall defect, which is the objective function to be minimized, is formulated as:

$$G=\frac{1}{V_t}\int_{V_s} w\, dV_s; w=\begin{cases} 1 & -22°C<T \quad \text{interior to the target region} \\ 0 & T \le -22°C \quad \text{interior to the target region} \\ 1 & T \le -22°C \quad \text{exterior to the target region} \\ 0 & -22°C<T \quad \text{exterior to the target region} \end{cases} \tag{6}$$

where V_S is the volume of the entire simulated domain (including both the target and external regions), V_t is the volume of the target region, and w is a spatial weight defect function, determined by the local temperature distribution. The tool developed in this study is based on the underlying assumption that displacement of a cryoprobe is considered to be an improvement if the value of the objective function, G, decreases. For the current study, prostate models are defined with uniform spatial grid spacing of 1 mm, and a tri-linear interpolation method is used to generate a uniform 1 mm temperature field from the variable grid size temperature data.

Bioheat transfer simulations start with a maximum value for the objective function. Initially, the entire defect is internal to the target domain, and its value decreases with the increasing size of the frozen region. Eventually, as the freezing process progresses, an increasing external defect develops. There is a balance point in which the total defect reaches a minimum; that is the ideal point of termination of the simulated cryoprocedure [7]. The final defect value is the parameter used to quantify the quality of the specific cryoprobe layout.

2.4. Planning Procedure

While the implementation of the planning algorithms discussed above may take numerous different forms—depending upon the clinical application, hardware selection, target shape, and the tissue to be treated—the current proof-of-concept study takes a three-step sequential approach for planning: (1) model selection of the target region from a model bank, (2) cryoprobe layout planning based on bubble packing, and (3) verification of planning by a bioheat transfer simulation. The prostate model was selected from the five available models reconstructed from ultrasound imaging in previous studies [22,26]. Developing techniques for real-time model reconstruction based on ultrasound imaging is the subject matter of parallel efforts by the authors, and is beyond the scope of the current study. Next, the proposed method generates boundary bubbles on the model boundaries, followed by seeding bubbles that represent cryoprobes within the target region (Section 2.1). The motion of these bubbles is simulated until they reach a force-equilibrium configuration (Section 2.1). A numerical grid is then generated for the particular model shape and the cryoprobe layout (Section 2.2). Finally, a single bioheat transfer simulation is executed (Section 2.2), while the objective function (Section 2.3) is routinely computed, until the point of minimum defect is reached. For simplicity of the current analysis, it is assumed that all cryoprobes are operated simultaneously. At the end of that process, simulation results are saved and compiled for further analysis, as discussed below.

Following the conclusions from previous studies [23], no additional planning steps are taken in order to further decrease the objective function value, which would be required in the force-field analogy algorithm [7]. While the number of cryoprobes was manually selected for analysis and discussion purposes, it is straightforward to search for the optimal number of cryoprobes based on defect results. However, comparing different planning layouts may require additional criteria—as discussed below—in order to reach a sound clinical decision of the best layout.

3. Results and Discussion

The advantages of variable insertion depth placement are discussed first in this section, in comparison with prior bubble-packing-based planning schemes; this comparison is performed on the largest reconstructed prostate model (model D, Table 2 [22]; see [11] for additional information on model reconstruction). Subsequently, the discussion is shifted to the unique characteristics of variable insertion depth planning, based on five prostate models.

3.1. Advantages of variable insertion depth over prior planning schemes

Using model D, four different cases have been analyzed: (1) uniform insertion depth with 25 mm-long cryoprobes, (2) pullback with 25 mm-long cryoprobes, (3) variable insertion depth with 25 mm-long cryoprobes, and (4) variable insertion depth with 35 mm-long cryoprobes; the cryoprobe length refers to the active surface for cooling, and the 35 mm length is related to a recent hardware development. Representative final bubble layouts for these four cases, each using eight cryoprobes, are displayed in Fig. 1. Note that a method for determining optimal insertion depth for Cases 1 and 2 has been presented elsewhere [24,25], and is associated with the geometry of the target region.

Planning results for the above cases with an overall number of cryoprobes ranging from 4 to 20 are displayed in Fig. 2, where current clinical procedures frequently use up to 14 cryoprobes and the number 20 was chosen as an upper limit. Due to their superior cooling power, it can be seen that the application of the 35 mm cryoprobe shortens the surgical duration. However, when six or more cryoprobes are used, the 35 mm cryoprobe case has the largest defect region. A clear trend is observed when ten or more cryoprobes are used, where Case 3 (25 mm probe, variable insertion depth) is superior in terms of the total defect region, followed by Cases 2, 1, and 4, respectively. An inverse trend is observed for the duration of the simulated cryoprocedure, with the exception of the pullback procedure (which requires two cycles of freezing). Based on Fig. 2 alone, variable insertion depth placement appears superior to both uniform insertion depth placement and the pullback procedure.

In order to further study the quality of planning for the four cases, Fig. 3 displays the resulting temperature fields for each case, using 14 cryoprobes on prostate model D, in three orthogonal cross-sectional views: transverse (perpendicular to the direction of cryoprobe insertion), coronal (top view when the patient lays on his back), and sagittal (side view). In general, a higher quality match is obtained between the isotherm for planning (−22°C) and the contour of the target region at the largest transverse cross section, in comparison with the other orthogonal cross sections, regardless of the number of cryoprobes or the technique of insertion. Given the elongated shape of the prostate, the circular nature of the urethra, and the ellipsoidal shape of the bubbles, this observation is not surprising. It is noted that clinicians frequently perform planning on similar representative transverse cross sections. While this practice may result in high quality planning for the particular transverse cross section chosen (as shown for Case 1 in Fig. 3), related planning results in other cross sections are often of lower quality.

The variable insertion depth results displayed in Fig. 3 suggest that cryoprobes can come quite close to one another. In the present form of the planning algorithm and in the most extreme case, cryoprobes are allowed to touch one another in the transverse cross-section, but are not permitted to overlap. However, due to the nature of the bubble motion in the bubble-packing method, the active surface of a cryoprobe—the portion of the cryoprobe enclosed within the bubble—cannot touch the active surface of an adjacent cryoprobe. The clinical application of a placement grid, where cryoprobes can only be placed at specific intervals on the transverse cross-section, is further discussed below.

Overall, it appears from Fig. 3 that either the pullback method (Case 2) or the variable insertion depth method with 25 mm-long cryoprobes (Case 3) provide the best outcome of planning, when results at all three cross sections are taken into consideration. As shown in Fig. 2, variable insertion depth placement offers both a smaller defective region and a shorter cryosurgical procedure. For example, the combined duration of both freeze cycles during the pullback case with 14 cryoprobes is 11.8 min, whereas it is only 5.1 min for the variable insertion depth case; the pullback case leads to a total defect area of 19.0%, whereas the variable insertion depth placement results in 15.2% defect. While the variable insertion depth technique offers a superior planning result for the given prostate model, the clinician's decision for the optimal planning may be affected by anatomical features in the vicinity of the treated region, such as nerve bundles, muscles, and adjacent organs.

The discussion now turns to a comparison between the shorter and longer cryoprobes, subject to variable insertion depth (Cases 3 and 4, respectively). While the 25 mm cryoprobes case (Case 3) offers better control and lower defect values, the 35 mm cryoprobes case (Case 4) allows for the use of fewer cryoprobes, while maintaining a similar duration of the procedure. For example, the simulated durations for Case 3 using 14 cryoprobes and Case 4 using 8 cryoprobes are 5.1 min and 8.3 min, respectively, while the respective defect values are 15.2% and 23.9% (Fig. 2). The clinician can use these values along with resulting temperature fields to decide if the superior control offered by the 25 mm cryoprobes outweighs the tissue injury and operational cost associated with increasing number of cryoprobe insertions to the target region.

3.2. Characteristics of variable insertion depth planning

Since the variable insertion depth technique with 25 mm-long cryoprobes provides superior planning results, even for as large of a target region as model D (Table 2), the remaining of the current study is focused on variable insertion depth cases using cryoprobes with active length of 25 mm. In addition, the application of 15 mm-long cryoprobes is also studied, for comparison purposes with prior hardware developments and corresponding studies.

Variable insertion-depth planning has been studied on five reconstructed prostate models, as listed in Table 2, having an average volume of 49.3±19.5 ml and an average length of 46.3±6.0 mm. Also listed in Table 2 is the distance from the apex of the prostate to a plane dividing the prostate into two equal-volume sections; this distance is presented normalized with respect to the prostate length. This value provides an indication of the relative "chestnut shape" of the prostate in the direction of cryoprobe insertion, and it ranges from 0.51 (relatively symmetric) to 0.62 (more pronounced chestnut shape). Finally, the average cross sectional area of the prostate in the direction of cryoprobe insertion is also presented, ranging from 618 mm^2 to 1391 mm^2 for the particular models. The variability in shape and size of the models used in the current study allows for a detailed evaluation of the variable insertion depth planning technique. Note that models B and D may exceed the typical candidate size for prostate cryosurgery.

Compared with uniform insertion depth, variable insertion depth placement consistently leads to a smaller defect area when 25 mm cryoprobes are used, as can be seen for prostate models A and B in Fig. 4. For a large number of cryoprobes, variable insertion depth with 15 mm cryoprobes further decreases the overall defect. However, for a small number of cryoprobes, the 25 mm-long cryoprobes result in superior planning due to the insufficient cooling power of a 15 mm-long cryoprobes.

As an example for the effect of a larger number of shorter cryoprobes, the case of 12 cryoprobes applied to prostate model A is discussed (Fig. 4). Here, defect values of 25.1% and 18.7% are observed for the 25 mm and 15 mm cryoprobe applications, respectively. The lower defect for shorter cryoprobes can be explained by analyzing the resulting temperature fields at the end of planning (i.e., at the point of minimum defect), as displayed in Fig. 5. As shown there, a large local defect area is found in the upper portion of the prostate model when the 25 mm cryoprobes are used (Case 5). This can be explained by the proximity of the urethra to the upper contour of the prostate, where the bubbles associated with the 25 mm cryoprobes are too large to fit into that gap. For the 15 mm case (Case 6), smaller bubbles are better packed in the same space, reducing the local defect. While Fig. 5 suggests that the 15 mm-long cryoprobe case results in smaller overall defect, its freezing duration is predicted to last 6.8 min, as compared to only 3.5 min for the 25 mm case. In order to reduce the duration of the freeze cycle of the 15 mm case, one alternative is to add more cryoprobes, as illustrated with Case 7 in Fig. 5, where the predicted duration of the procedure is reduced to 3.3 min for 20 cryoprobes. Here the increased number of cryoprobes decreased the defect by 5.5%.

A notably different trend is observed when comparing the defect results for the different active lengths for prostate model B, as shown in Fig. 4(bottom). There is an insignificant difference in the defect values for the cases using ten or more cryoprobes. In fact, the 25 mm case yields lower defect values for both the 10 and 12 cryoprobe cases, with considerably shorter predicted surgical durations. In Fig. 6, the resulting temperature field is shown for the cases of 12 cryoprobes having a length of 25 mm (Case 8) and 20 cryoprobes having a length of 15 mm (Case 9). Even when an excessive number of 20 cryoprobes is used, the 15 mm case shows only marginal improvement. Thus, for prostate model B, there appears to be little advantage for using the smaller sized cryoprobes. Comparing the results and trends for planning on prostate models A and B, it can be concluded that, while results can be rationalized for a specific model, making universal planning rules for all possible models is not feasible and individual computerized planning is in order.

The discussion now turns to the determination of an optimal number of cryoprobes. It has been previously reported that the low computational cost of the bubble-packing method may also permit optimization of the number of cryoprobes [18], with representative results listed in Table 2. A definite trend can be observed in Table 2, that both the defect region and simulated duration decrease with the increasing number of cryoprobes, for a given prostate model and a given cryoprobe length. The rates by which these values improve, however, decay with the increasing number of cryoprobes. Also listed in Table 2 is the percentage of the target region which is below three the key temperature isotherms of 0°C, −22°C, and −45°C. For all cases listed in Table 2, the additions of cryoprobes increases the respective volumes below the key isotherms, as could be expected due to the increase in cooling power and, thereby, increase in temperature gradients.

For the cases presented above, the typical runtime for bubble packing was consistently under one minute, using a 3.4 GHz Pentium 4 machine with 1.5 GB of memory. Based on a prior study [17], the bioheat transfer simulations are expected to have runtimes between one and five minutes. Results like those listed in Table 2 can potentially be used by the clinician

when determining the optimal number of cryoprobes in conjunction with the optimal cryoprobe active length for a given prostate model. The low computational cost of bubble packing-based planning enables such real-time application.

Finally, the placement grid effect on computerized planning is discussed, where the placement grid is a steel plate with an X–Y array of holes (typically at 5 mm intervals), which is used to assist the clinician in cryoprobe localization. For each of the cases listed in Table 2, an additional bioheat simulation was executed, after relocating (snapping) the cryoprobes so as to conform to the placement grid using the following rules: (i) select the placement grid location so as to minimize the average cryoprobe displacement, (ii) two cryoprobes cannot occupy the same grid point, and (iii) cryoprobes cannot be placed outside of the prostate domain. The defect value resulting from snapping the cryoprobes to the placement grid holes, along with the change in the defect value with respect to the original locations, are listed in the right two columns of Table 2. For most cases, a relatively small increase in defect value is observed after snapping. The largest changes are seen with cases using prostate model C, due to its small size.

While evaluating these results it should be noted that a placement grid is routinely used in prostate operations, which represents an incremental step in terms of the computation complexity. However, the authors do not see the application of a placement grid and manual cryoprobe insertion through its holes as the only alternative for cryoprobe insertion in the modern clinical arena. The authors envision the application of the robotic placement of cryoprobes, in which the optimal insertion path is selected for each cryoprobe on an individual basis.

4. Summary and Conclusions

As part of ongoing efforts to develop computerized planning tools for cryosurgery, a planning scheme for variable cryoprobe-insertion depth has been presented. This scheme is a modification of a pervious scheme, employing the bubble-packing method to evenly distribute cryoprobes within the target domain. The scheme was tested on five different prostate models, reconstructed from ultrasound images in previous studies. Developing techniques for real-time model reconstruction, based on ultrasound imaging, is the subject matter of parallel effort by the authors. Nevertheless, the planning technique presented here is general, suitable for any 3D shape of the target region, and independent of the reconstruction technique. The quality of planning was evaluated through the use of bioheat transfer simulations and the concept of defect region.

The defect region is defined as tissue outside of the target region with temperatures below an isotherm threshold for planning, or an area within the target region with temperatures above the same temperature threshold. Mathematically, there should always be a point in time at which the overall defect region reaches a minimum; this is the suggested point for termination of the cryoprocedure. The objective of the current study is not only to find the optimal point in time to terminate the cryoprocedure (i.e., a local minimum) but also to find which cryoprobe layout, out of all studied layouts, yields the lowest value of defect (i.e., the global minimum). While the overall defect was the overriding parameter for planning at the current proof-of-concept stage of development, one can increase the level of sophistication of the target function to give different weights to defects at different locations. The target function may be further enhanced to incorporate clinical rules for cryoprobe placement, with the minimum distance between cryoprobes and the urethral wall as an example in the current study.

Planning results for variable insertion depth of cryoprobes were compared with results using both a uniform insertion depth and the pullback procedure, for a range of cryoprobes

number. When enough cryoprobes were used to sufficiently cryotreat the target domain, the variable insertion depth technique proved to be superior to the other placement methods tested.

The effect of the cryoprobe active length on planning was investigated (15 mm, 25 mm, and 35 mm) for the variable insertion-depth strategy. It was concluded that the shorter cryoprobes are likely to lead to a smaller defect region, provided that enough cryoprobes are used. In return, shorter cryoprobes require longer procedure durations. In general, the benefit from using the shorter cryoprobes appeared to be greatest when they were applied to smaller prostate models. Nevertheless, general rules often cannot be drawn (considering variations in both prostate shape and surrounding anatomical features), and an interactive planning scheme is likely to lead to better planning decisions. The bubble-packing method is rapid enough to enable such interactive work in a clinically relevant time period.

Acknowledgments

This project is supported by the National Institute of Biomedical Imaging and Bioengineering (NIBIB) – NIH, grant No. R01-EB003563-01,02,03,04. The authors would like to thank Dr. Aaron Fenster of the Robarts Imaging Institute, London, Canada, for providing ultrasound images. The authors would also like to thank Dr. Ralph Miller of Allegheny General Hospital, Pittsburgh, Pennsylvania, for clinical advice.

References

1. Altman, PL.; Dittmer, DS. Respiration and Circulation, Federation of American Societies for Experimental Biology (Data Handbook). Bethesda, MD: 1971.
2. Baissalov R, Sandison GA, Donnelly BJ, Saliken JC, McKinnon JG, Muldrew K, Rewcastle JC. A semi-empirical treatment planning model for optimization of multiprobe cryosurgery. Phys. Med. Biol 2000;45:1085–1098. [PubMed: 10843092]
3. Baissalov R, Sandison GA, Reynolds D, Muldrew K. Simultaneous optimization of cryoprobe placement and thermal protocol for cryosurgery. Phys. Med. Biol 2001;46:1799–1814. [PubMed: 11474926]
4. Cooper IS, Lee A. Cryostatic congelation: a system for producing a limited controlled region of cooling or freezing of biological tissues. J. Nerve Mental Dis 1961;133:259–263.
5. Gage AA. Cryosurgery in the treatment of cancer. Surg. Gynecol. Obstet 1992;174:73–92. [PubMed: 1729758]
6. Keanini RG, Rubinsky B. Optimization of multiprobe cryosurgery. J. Heat Trans.-T. ASME 1992;114:796–802.
7. Lung DC, Stahovich TF, Rabin Y. Computerized planning for multiprobe cryosurgery using a force-field analogy. Comp. Meth. Biomech. Biomed. Eng 2004;7(2):101–110.
8. Onik GM, Cohen JK, Reyes GD, Rubinsky B, Chang ZH, Baust J. Transrectal ultrasound-guided percutaneous radical cryosurgical ablation of the prostate. Cancer 1993;72(4):1291–1299. [PubMed: 7687922]
9. Onik GM, Gilbert JC, Hoddick W, Filly R, Callen P, Rubinsky B, Farrel L. Sonographic monitoring of hepatic cryosurgery in an experimental animal model. Am. J. Roentgenol 1985;144(5):1043–1047. [PubMed: 3885689]
10. Pennes HH. Analysis of tissue and arterial blood temperatures in the resting human forearm. J. App. Phys 1948;1:93–122.
11. Rabin Y. Developing computerized tools for cryosurgery planning. 2007 http://www.me.cmu.edu/faculty1/rabin/RabinCryoPlan.htm.
12. Rabin Y, Korin E. An efficient numerical solution for the multidimensional solidification (or melting) problem using a microcomputer. Int. J. Heat Mass Tran 1993;36(3):673–683.
13. Rabin Y, Shitzer A. Numerical solution of the multidimensional freezing problem during cryosurgery. J. Biomech. Eng.-T. ASME 1998;120(1):32–37.

14. Rabin Y. A general model for the propagation of uncertainty in measurements into heat transfer simulations and its application to cryobiology. Cryobiology 2003;46(2):109–120. [PubMed: 12686201]
15. Rabin Y, Lung DC, Stahovich TF. Computerized planning of cryosurgery using cryoprobes and cryoheaters. Technol. Cancer Res. T 2004;3(3):227–243.
16. Rossi MR, Rabin Y. Experimental verification of numerical simulations of cryosurgery with application to computerized planning. Phys. Med. Biol 2007;52:4553–4567. [PubMed: 17634650]
17. Rossi MR, Tanaka D, Shimada K, Rabin Y. An efficient numerical technique for bioheat simulations and its application to computerized cryosurgery planning. Comput. Meth. Prog. Bio 2007;85(1):41–50.
18. Rossi MR, Tanaka D, Shimada K, Rabin Y. Computerized planning of cryosurgery using bubble packing: An experimental validation on a phantom material. The International Journal of Heat and Mass Transfer 2008;51:5671–5678.
19. Rubinsky B, Gilbert JC, Onik GM, Roos MS, Wong STS, Brennan KM. Monitoring cryosurgery in the brain and the prostate with proton NMR. Cryobiology 1993;30:191–199. [PubMed: 8319488]
20. Schulz T, Puccini S, Schneider JP, Kahn T. Interventional and intraoperative MR: review and update of techniques and clinical experience. Eur. Radiol 2004;14(12):2212–2227. [PubMed: 15480689]
21. Shimada, K. PhD thesis. Cambridge, MA: Massachusetts Institute of Technology; 1993. Physically-Based Mesh Generation: Automated Triangulation of Surfaces and Volumes via Bubble-Packing.
22. Tanaka D, Rossi MR, Shimada K, Rabin Y. Towards intra-operative computerized planning of prostate cryosurgery. Int. J. Med. Robot. Comp 2007;3:10–19.
23. Tanaka D, Shimada K, Rabin Y. Two-phase computerized planning of cryosurgery using bubble-packing and force-field analogy. J. Biomech. Eng.-T. ASME 2006;128(1):49–58.
24. Tanaka D, Shimada K, Rossi MR, Rabin Y. Cryosurgery planning using bubble packing in 3D. Comp. Meth. Biomech. Biomed. Eng 2008;11(2):113–121.
25. Tanaka D, Shimada K, Rossi MR, Rabin Y. Computerized planning of prostate cryosurgery with pullback operation. Comput. Aided Surg 2008;13(1):1–13. [PubMed: 18240050]
26. http://www.andrew.cmu.edu/user/yr25/ProstateModelReconstructionF.htm

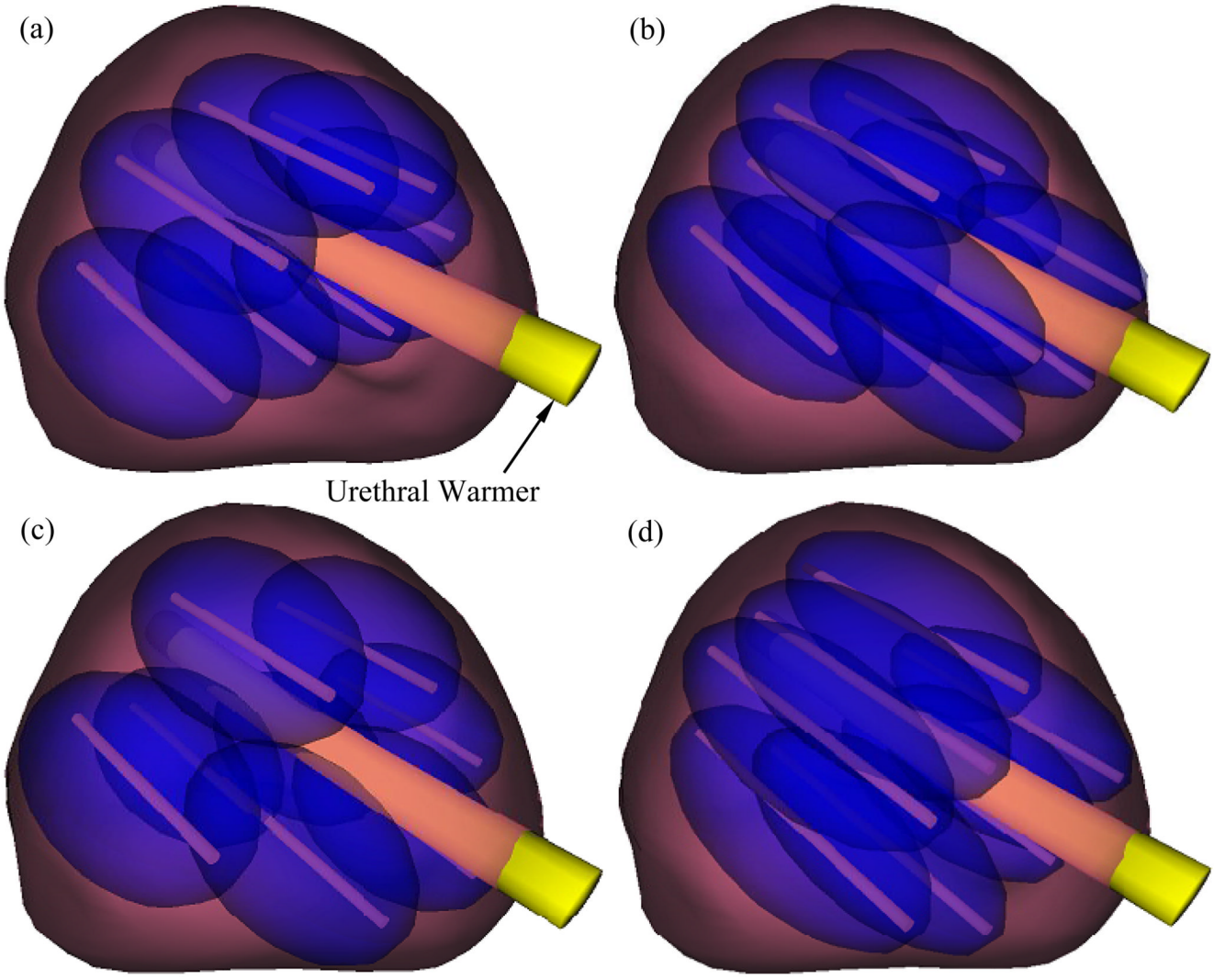

Figure 1.
Representative results for planned cryoprobe layouts, packing eight bubbles in prostate model D (Table 2), subject to: (a) a uniform insertion depth with 25 mm-long cryoprobes, (b) a pullback procedure with 25 mm-long cryoprobes, (c) a variable insertion depth with 25 mm-long cryoprobes, and (d) a variable insertion depth with 35 mm-long cryoprobes; cryoprobe length refers to its active cooling surface.

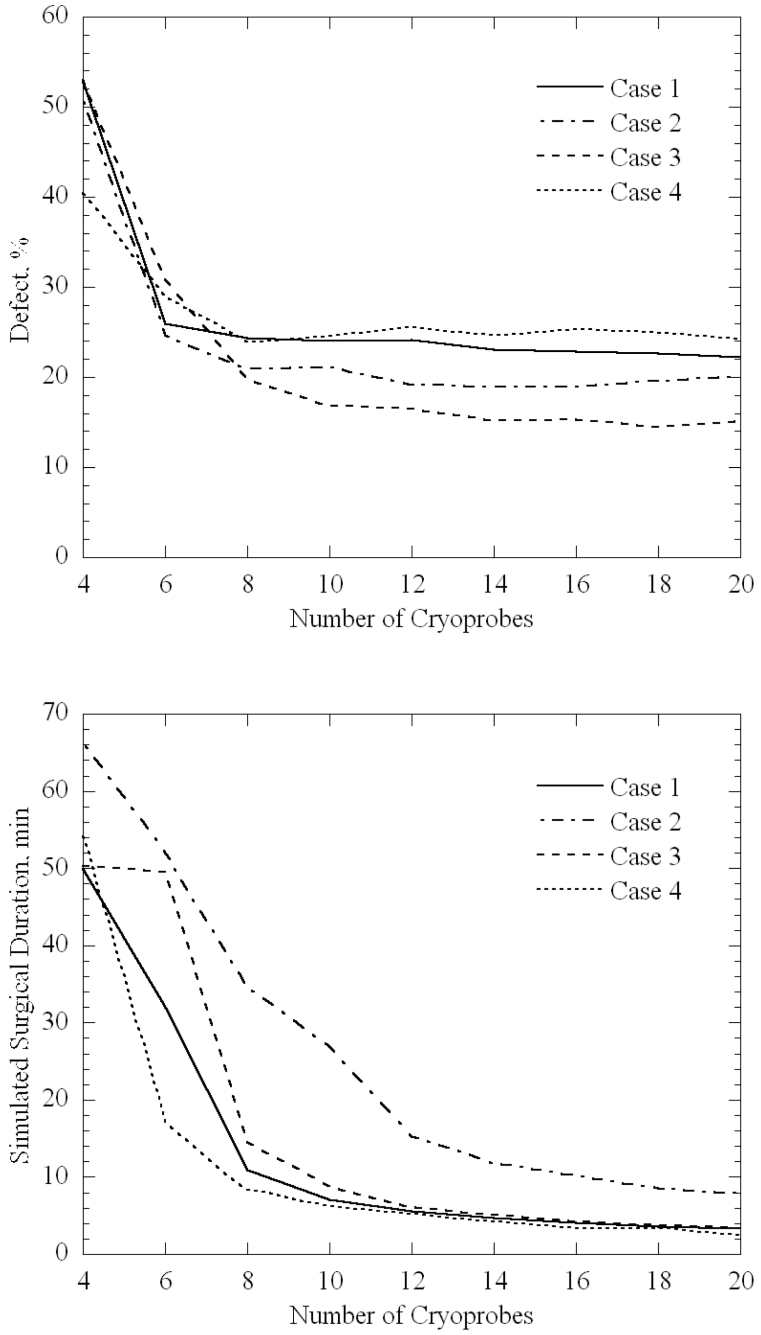

Figure 2.

Planning results for prostate model D: (1) a uniform insertion depth with 25 mm-long cryoprobes, (2) a pullback procedure with 25 mm-long cryoprobes, (3) a variable insertion depth with 25 mm-long cryoprobes, and (4) a variable insertion depth with 35 mm-long cryoprobes; the top figure displays the defect value for optimum layout, while the bottom figure displays the simulated duration of the cryoprocedure at the planned layout.

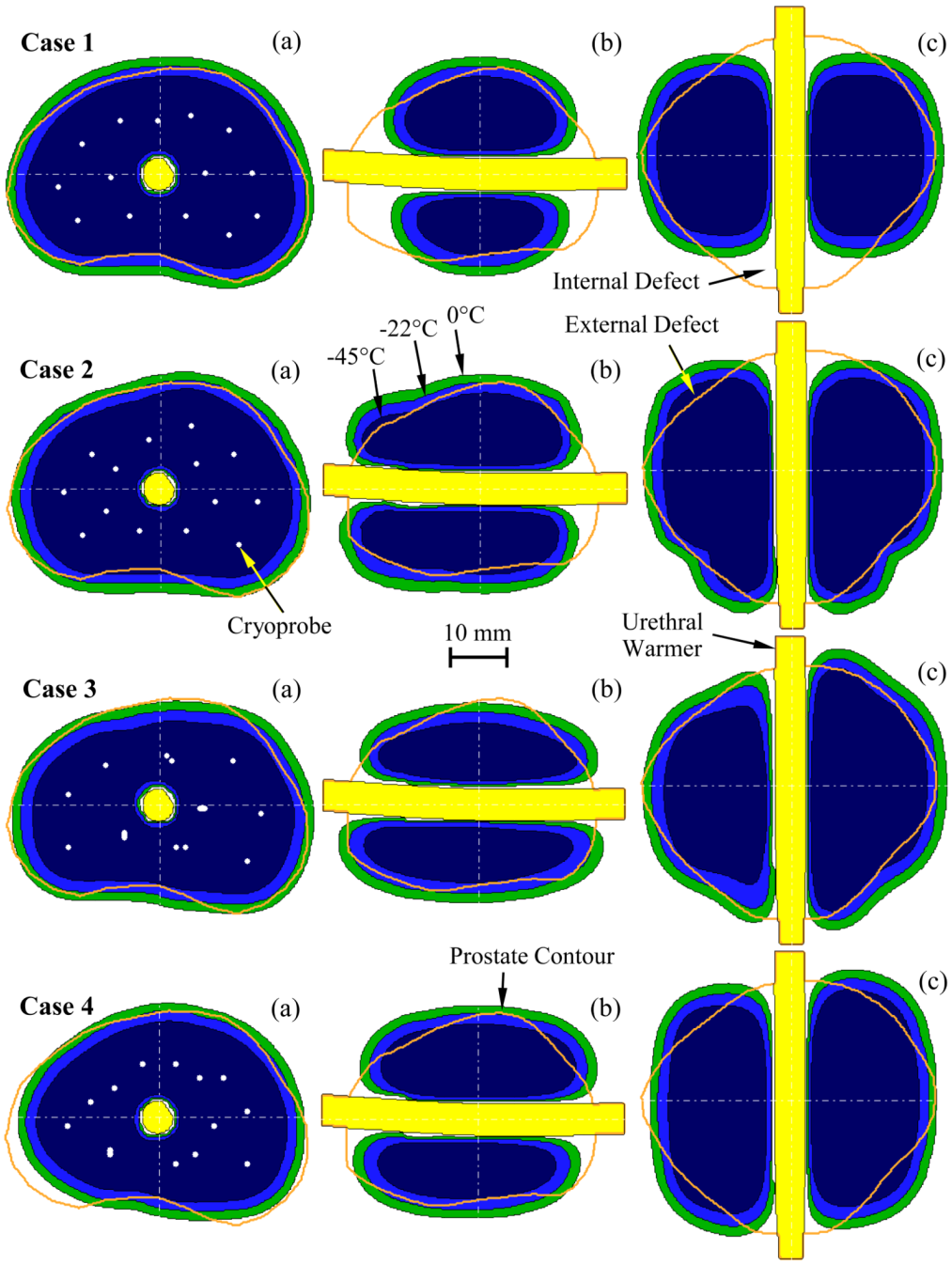

Figure 3.

Resulting temperature field in representative orthogonal cross sections of prostate model D (a: transverse, b: sagittal, and c: coronal), for four cases of planning, each using 14 cryoprobes: (1) a uniform insertion depth, having a 25 mm-long active surface—total defect of 28.4% ; (2) a pullback procedure using all 14 cryoprobes in the first stage and seven cryoprobes in the second stage, having a 25 mm-long active surface—total defect of 19.0%; (3) a variable insertion depth, having a 25 mm-long active surface—total defect of 15.2%; and (4) a variable insertion depth, having a 35 mm-long active surface—total defect of 24.7%.

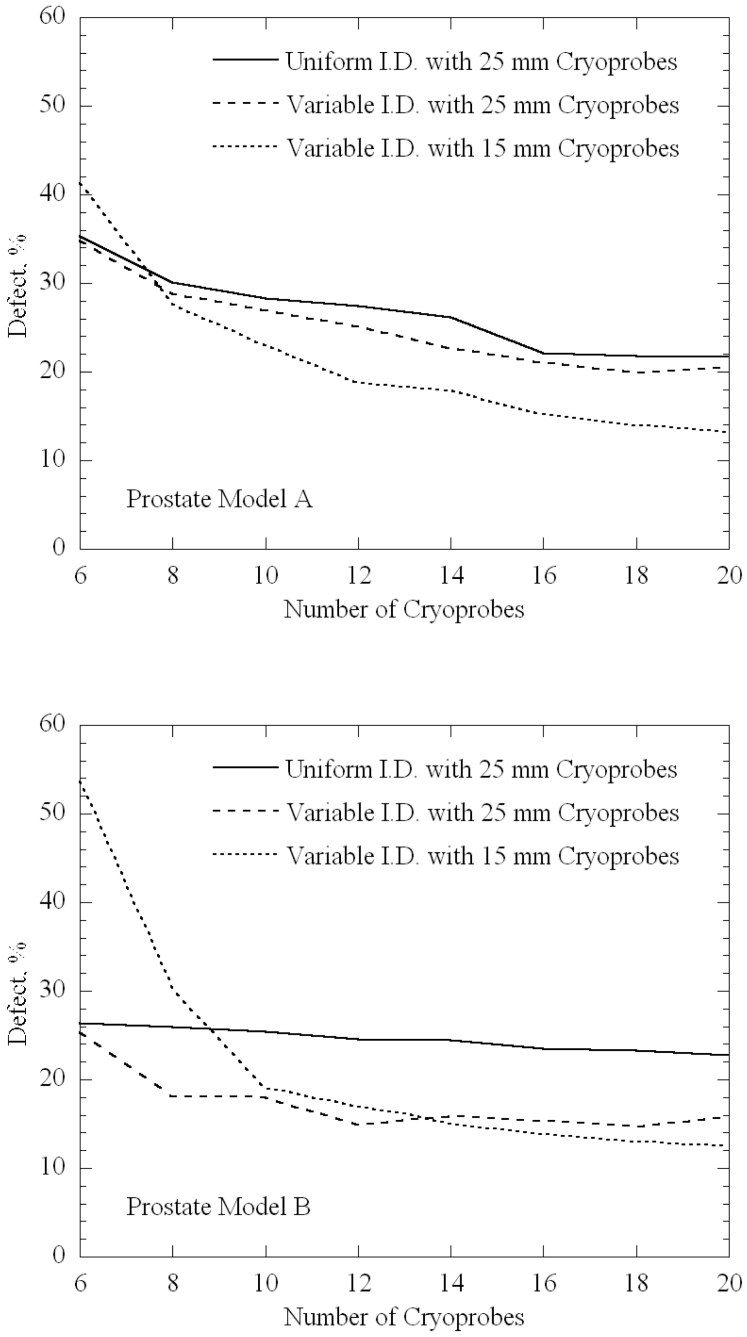

Figure 4.

Overall defect for optimal planning on prostate models A (top) and B (bottom) subject to: (1) a uniform insertion depth with 25 mm-long cryoprobes, (2) a variable insertion depth with 25 mm-long cryoprobes, and (3) a variable insertion depth with 15 mm-long cryoprobes.

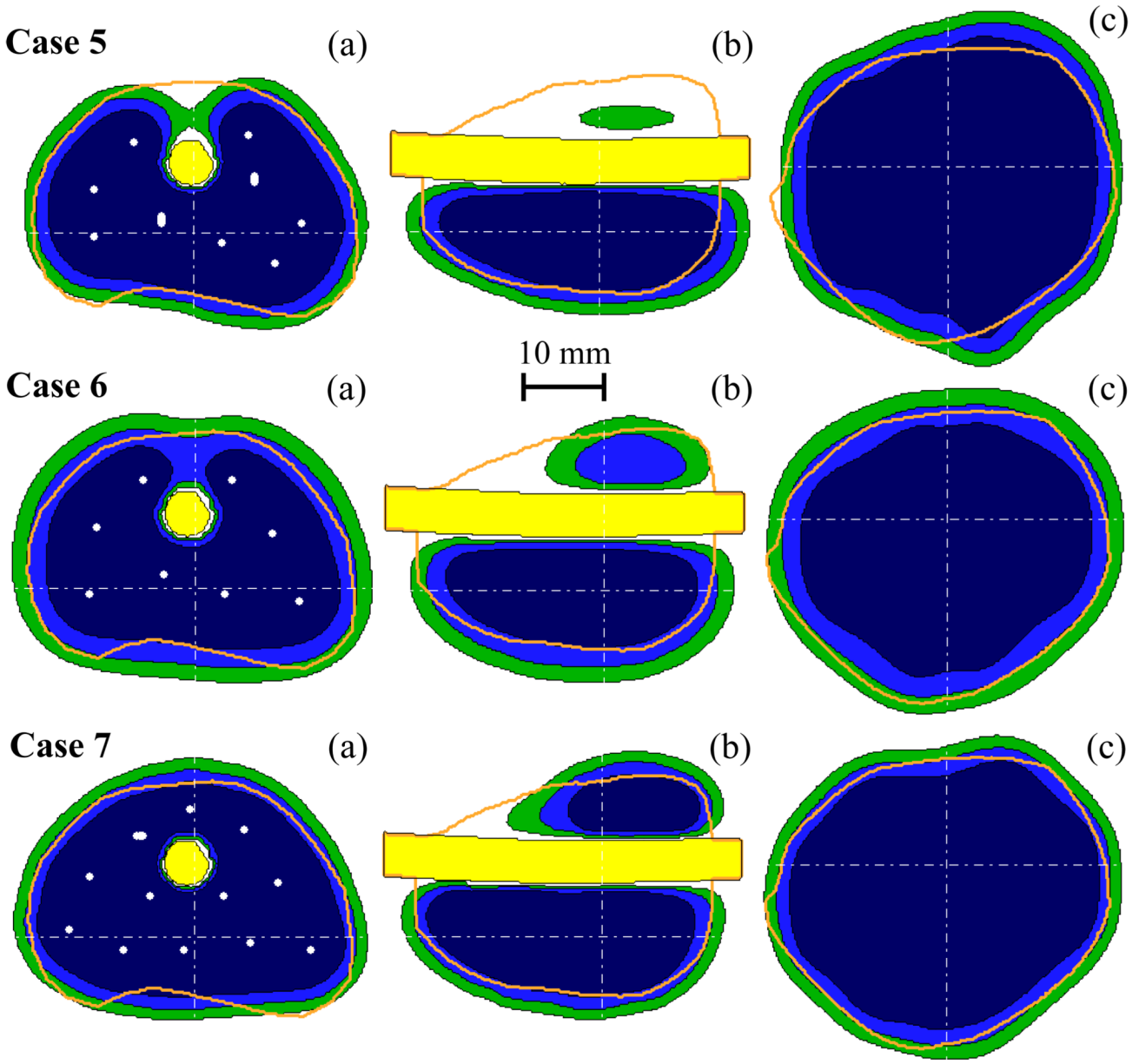

Figure 5.
Resulting temperature field in representative orthogonal cross sections of prostate model A (a: transverse, b: sagittal, and c: coronal) for three planning cases using variable insertion depths: (5) 12 cryoprobes, having a 25 mm-long active surface—total defect of 25.1%; (6) 12 cryoprobes, having a 15 mm-long active surface—total defect of 18.7%; and (7) 20 cryoprobes, having a 15 mm-long active surface—total defect of 13.2%.

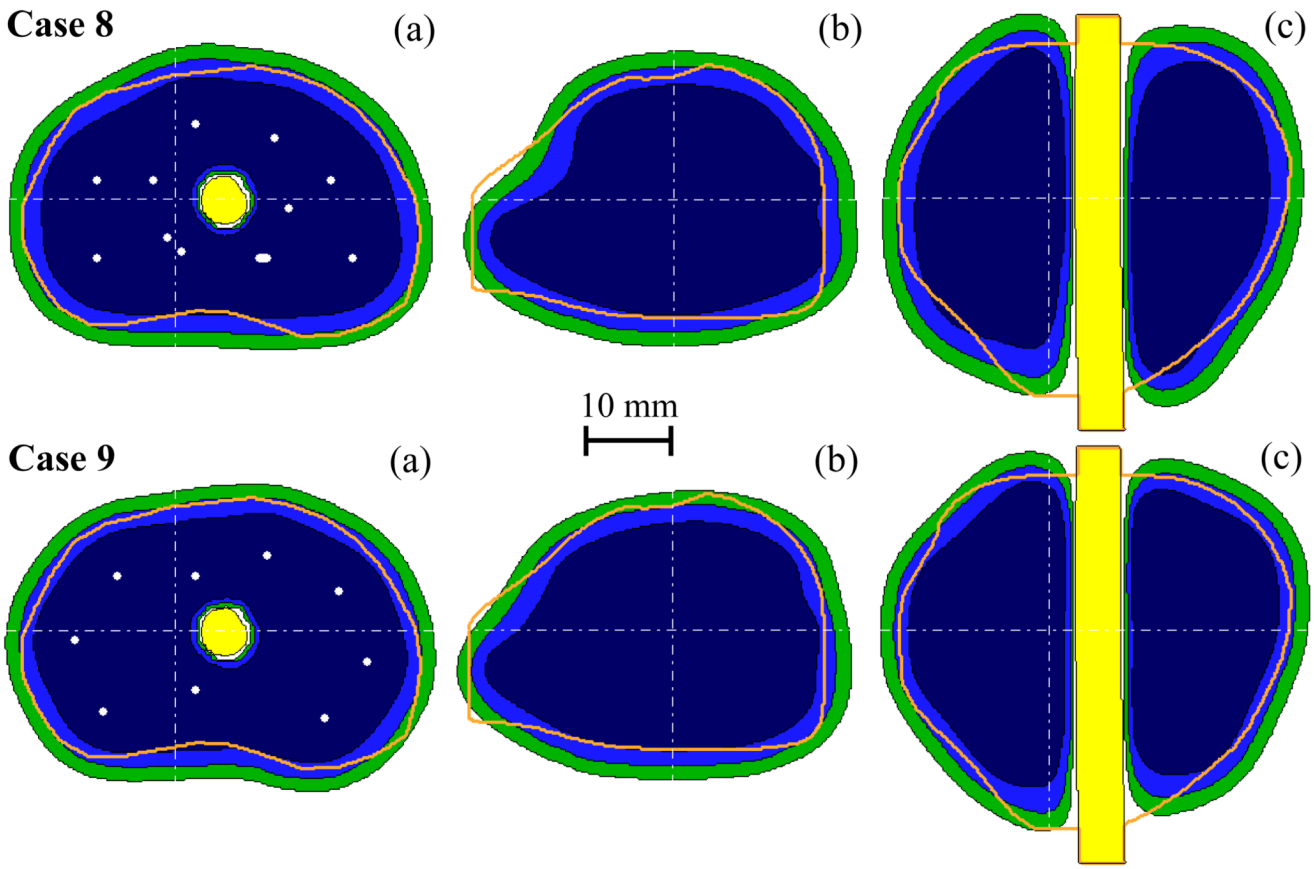

Figure 6.
Resulting temperature field in representative orthogonal cross sections of prostate model B (a: transverse, b: sagittal, and c: coronal) for two cases of planning using variable insertion depths: (8) 12 cryoprobes, having a 25 mm-long active surface—total defect of 14.9%; and (9) 20 cryoprobes, having a 15 mm-long active surface—total defect of 12.4%.

Table 1

Representative thermophysical properties of biological tissues used in the current study [1,15]

Thermophysical Property	Value	
Thermal conductivity, k, W/m-K	0.5	273K < T
	15.98 – 0.0567×T	251K < T < 273K
	$1005\times T^{-1.15}$	T< 251K
Volumetric specific heat, C, MJ/m^3-K	3.6	273K < T
	880 – 3.21×T	265K < T < 273K
	2.017×T – 505.3	251K < T < 265K
	0.00415×T	T < 251K
Blood perfusion, w_bC_b, kW/m^3-K	40	273K < T
	0	T ≤ 273K

Table 2

Summary of prostate model dimensions [22] and planning results, using 15 mm-long cryoprobes at variable insertion depths, where V_P is the prostate volume; L_P is the prostate length; L_{V2} is the distance from the apex of the prostate to a plane dividing the prostate into two sections of identical volume; A_C is the average cross sectional area of the prostate in the direction parallel to cryoprobe insertion; N_P is the number of cryoprobes; D_M is the minimum defect; t_D is the simulated time at which the minimum defect is reached; I_0, I_{-22}, and I_{-45} represent the percentage of the target region with temperatures below the 0°C, −22°C, and −45°C, respectively; D_G is the defect value when a 5 mm × 5 mm placement grid is used; and ΔD is the difference between D_M and D_G.

Prostate Model	N_P	D_M, %	t_D, min	I_0, %	I_{-22}, %	I_{-45}, %	D_G, %	ΔD, %
A	6	41.2	27.9	81.2	61.2	31.1	42.5	1.2
	8	27.7	17.6	92.3	78.1	43.9	27.4	−0.3
	10	23.0	9.8	94.4	83.4	51.7	23.1	0.1
V_P = 44.4 ml	12	18.7	6.8	96.5	86.0	55.6	21.5	2.8
L_P = 44.5 mm	14	17.9	5.0	96.3	85.9	58.8	19.5	1.6
L_{V2} = 26 mm	16	15.2	4.3	97.4	89.3	64.1	17.7	2.5
L_{V2}/L_P = 0.58	18	14.0	3.8	98.1	91.0	67.3	15.4	1.5
A_C = 998 mm^2	20	13.2	3.3	97.9	90.4	68.6	16.6	3.3
B	6	53.6	45.6	76.8	46.4	18.0	51.0	−2.6
	8	30.3	40.8	92.3	71.4	32.9	32.2	1.9
	10	19.0	23.7	97.2	85.9	46.2	22.9	4.0
V_P = 62.8 ml	12	16.9	11.4	97.7	87.1	51.9	19.9	3.0
L_P = 49.9 mm	14	15.0	8.2	98.2	89.1	57.2	17.9	2.9
L_{V2} = 28 mm	16	13.9	6.7	98.2	90.2	61.1	16.6	2.7
L_{V2}/L_P = 0.56	18	13.0	5.7	98.7	91.7	65.1	13.0	0.1
A_C = 1259 mm^2	20	12.4	4.8	98.8	92.1	68.0	15.7	3.2
C	6	36.2	11.5	87.5	69.2	34.2	36.9	0.7
	8	27.6	5.5	91.2	77.8	44.2	32.7	5.1
	10	23.2	4.2	93.9	83.3	52.8	29.8	6.6
V_P = 23.0 ml	12	20.2	3.3	95.3	84.8	56.8	25.1	4.9
L_P = 37.2 mm	14	17.0	2.8	96.3	87.0	61.7	27.3	10.3
L_{V2} = 23 mm	16	16.8	2.3	96.6	88.3	66.5	23.8	7.0
L_{V2}/L_P = 0.62	18	15.5	2.1	97.0	89.5	69.2	24.2	8.8
A_C = 618 mm^2								

Prostate Model	N_P	D_M, %	t_D, min	I_0, %	I_{-22}, %	I_{-45}, %	D_G, %	ΔD, %
	20	14.8	1.9	97.6	91.9	73.4	24.4	9.6
D V_P = 73.6 ml L_P = 52.9 mm L_{V2} = 27 mm L_{V2}/L_P = 0.51 A_C = 1391 mm^2	6	58.3	53.3	69.4	41.7	15.6	58.4	0.1
	8	33.5	52.7	91.1	66.7	29.7	32.2	−1.3
	10	18.5	30.2	95.8	84.4	44.6	22.9	4.4
	12	16.3	15.1	97.0	87.7	51.8	19.9	3.7
	14	14.7	10.6	97.6	89.0	56.6	17.9	3.2
	16	14.7	7.7	97.3	89.0	60.2	17.7	3.0
	18	13.3	6.4	97.8	90.2	63.5	16.3	3.0
	20	12.5	5.7	98.7	91.7	66.9	15.3	2.9
E V_P = 42.8 ml L_P = 47.0 mm L_{V2} = 28 mm L_{V2}/L_P = 0.60 A_C = 911 mm^2	6	40.3	31.1	82.6	60.9	27.9	42.7	2.4
	8	30.5	15.4	89.9	75.8	42.4	35.9	5.4
	10	23.8	8.8	93.0	81.8	49.6	26.3	2.5
	12	21.2	6.2	94.6	83.3	53.9	23.0	1.8
	14	18.8	5.2	96.6	86.4	59.0	21.6	2.8
	16	15.9	4.3	96.9	89.0	63.5	18.5	2.6
	18	15.9	3.6	96.6	88.6	65.4	20.6	4.7
	20	16.2	3.3	97.4	89.8	68.7	19.8	3.6